OXFORD

Human Molecular Genetics, 2016, Vol. 25, No. 1 109–122

doi: 10.1093/hmg/ddv453
Advance Access Publication Date: 5 November 2015
Original Article

ORIGINAL ARTICLE

14-3-3 Proteins regulate mutant LRRK2 kinase activity and neurite shortening

Nicholas J. Lavalley, Sunny R. Slone, Huiping Ding, Andrew B. West and Talene A. Yacoubian*

Department of Neurology, Center for Neurodegeneration and Experimental Therapeutics, University of Alabama at Birmingham, Birmingham, AL 35294, USA

*To whom correspondence should be addressed at: Department of Neurology, Center for Neurodegeneration and Experimental Therapeutics, University of Alabama at Birmingham, Civitan International Research Center 560D, 1719 6th Avenue South, Birmingham, AL 35294, USA. Tel: +1 2059967543; Fax: +1 2059966580; Email: tyacoub@uab.edu

Abstract

Mutations in *leucine-rich repeat kinase 2 (LRRK2)* are the most common known cause of inherited Parkinson's disease (PD), and *LRRK2* is a risk factor for idiopathic PD. How LRRK2 function is regulated is not well understood. Recently, the highly conserved 14-3-3 proteins, which play a key role in many cellular functions including cell death, have been shown to interact with LRRK2. In this study, we investigated whether 14-3-3s can regulate mutant LRRK2-induced neurite shortening and kinase activity. In the presence of 14-3-3θ overexpression, neurite length of primary neurons from BAC transgenic G2019S-LRRK2 mice returned back to wild-type levels. Similarly, 14-3-3θ overexpression reversed neurite shortening in neuronal cultures from BAC transgenic R1441G-LRRK2 mice. Conversely, inhibition of 14-3-3s by the pan-14-3-3 inhibitor difopein or dominant-negative 14-3-3θ further reduced neurite length in G2019S-LRRK2 cultures. Since G2019S-LRRK2 toxicity is likely mediated through increased kinase activity, we examined 14-3-3θ's effects on LRRK2 kinase activity. 14-3-3θ overexpression reduced the kinase activity of G2019S-LRRK2, while difopein promoted the kinase activity of G2019S-LRRK2. The ability of 14-3-3θ to reduce LRRK2 kinase activity required direct binding of 14-3-3θ with LRRK2. The potentiation of neurite shortening by difopein in G2019S-LRRK2 neurons was reversed by LRRK2 kinase inhibitors. Taken together, we conclude that 14-3-3θ can regulate LRRK2 and reduce the toxicity of mutant LRRK2 through a reduction of kinase activity.

Introduction

Parkinson's disease (PD) is the second most common neurodegenerative disorder behind Alzheimer's disease. The standard treatment for PD, levodopa, helps ameliorate motor symptoms and has improved the morbidity and mortality associated with PD, yet patients still have increased mortality rates and greatly diminished quality of life compared with the healthy population (1,2). Additionally, the occurrence of levodopa induced dyskinesias and motor fluctuations points to the need for more effective treatments for PD. Although most PD cases occur sporadically, several genes can cause inherited forms of PD. Mutations in *leucine-rich repeat kinase 2 (LRRK2)* are the most common known genetic cause of PD with the G2019S mutation as the most common known pathogenic mutation (3–6). Patients with LRRK2 mutations tend to show a clinically identical disease phenotype as those with idiopathic PD (5,7). LRRK2 is also a risk factor for idiopathic PD in genome-wide association studies (8–10).

LRRK2 protein contains a leucine-rich repeat domain, a Ras-of-complex domain, a C-terminus of ROC domain, a kinase domain, and a WD40-like domain. Current evidence points to increased kinase activity as a key mechanism for LRRK2 neurotoxicity (11–15). The physiological function of LRRK2 remains to be elucidated. Recent studies suggest that LRRK2 affects neurite outgrowth through regulation of tubulin (16–18). Several pathogenic *LRRK2* mutations cause a reduction in neurite growth, and inhibiting kinase activity can reverse this effect (19–23).

Received and Revised: September 28, 2015. **Accepted:** October 26, 2015

How LRRK2 function is regulated in health and disease is not well understood. LRRK2 protein interacts with 14-3-3s (24–26), a family of seven conserved proteins that participate in many cellular functions with an important role in cell survival (27). 14-3-3s mediate their function by interaction with binding proteins to alter enzymatic activity, subcellular localization or stability (28,29). Alterations in 14-3-3 expression or phosphorylation are observed in alpha-synuclein (αsyn)-based PD models and in human PD (30–33), and transcriptional analysis of PD samples has shown 14-3-3s as a critical hub of dysregulated proteins in PD (34). 14-3-3 overexpression is protective, while 14-3-3 inhibition promotes toxicity in rotenone, 1-methyl-4-phenyl-1,2,3, 6-tetrahydropyridine (MPTP) and αsyn models (32,35,36).

14-3-3s interact with LRRK2 at several phosphorylated serine sites, serines 910, 935 and 1444 (25,26,37). Several pathogenic LRRK2 mutants have decreased interaction with 14-3-3s (25,26), suggesting the importance of 14-3-3s in regulating LRRK2 function and toxicity. Mutation of S910/S935 to alanine to disrupt the 14-3-3/LRRK2 interaction causes punctate, perinuclear redistribution of LRRK2 in HEK293 cells (26).

Here, we examine the effects of 14-3-3s on LRRK2 phosphorylation, kinase activity and regulation of neurite growth. We focus on the 14-3-3θ isoform, as this isoform interacts with LRRK2 protein (25,26) and has the broadest protective effect on several PD models (32).

Results

14-3-3s Regulate LRRK2 phosphorylation at serines 910 and 935

The interaction between 14-3-3s and LRRK2 is dependent on phosphorylation at S910 and S935 residues in LRRK2, and mutation of LRRK2 at either serine site to disrupt 14-3-3 binding causes redistribution of cytosolic LRRK2 (26). We investigated the effects of 14-3-3 inhibition on LRRK2 phosphorylation at these serine sites. Difopein (dimeric fourteen-three-three peptide inhibitor) is a high-affinity 14-3-3 competitive antagonist peptide that inhibits 14-3-3/ligand interactions by binding within the amphipathic groove of 14-3-3s without selectivity among the 14-3-3 isoforms (38). We first confirmed that difopein disrupts the interaction between 14-3-3s and LRRK2. Co-immunoprecipitation of endogenous 14-3-3s with wild-type LRRK2 was reduced in HEK293T cells co-transfected with LRRK2 and difopein tagged with enhanced yellow fluorescent protein (eYFP), when compared with control HEK293T cells co-transfected with LRRK2 and mutant difopein-eYFP that is unable to bind and inhibit 14-3-3s (38) (Fig. 1A). Mutant difopein-eYFP contains two mutations of acidic residues (D12 and E14) to lysine residues that block binding to 14-3-3s (38).

Binding of 14-3-3s to LRRK2 could prevent dephosphorylation of LRRK2 by protein phosphatase 1 (PP1) at S910 and S935 (39). We examined whether 14-3-3 inhibition by difopein altered LRRK2 phosphorylation at S910 or S935. Difopein caused a significant decrease in wild-type and G2019S-LRRK2 phosphorylation at both S910 and S935 in HEK293T cells compared with cells transfected with mutant difopein (Fig. 1B). Similarly, S935 phosphorylation of endogenous LRRK2 was decreased *in vivo* by 85% in hippocampal lysates from transgenic mice that express difopein-eYFP under the Thy1.2 promoter (40), when compared with nontransgenic littermates (Fig. 1C). The Thy1.2 promoter drove high difopein-eYFP expression in the cortex and hippocampus (Fig. 3C and E).

We then tested the effect of 14-3-3θ overexpression on S910 and S935 phosphorylation *in vitro* and *in vivo*. 14-3-3θ Overexpression caused a significant increase in S910 and S935 phosphorylation of wild type and G2019S-LRRK2 in HEK 293T cells (Fig. 1D). To examine the effects of 14-3-3θ overexpression *in vivo*, we took advantage of our recently created transgenic mouse that overexpresses HA-tagged 14-3-3θ under the Thy1.2 promoter. Two of the founder lines demonstrated high expression of HA-tagged 14-3-3θ in the cortex and hippocampus, with the M5 line showing particularly high levels of exogenous HA-tagged 14-3-3θ in the hippocampus (Fig. 2A–C). While HA-tagged 14-3-3θ expression increased over time in these mice due to the Thy1.2 promoter, expression was detected early postnatally in the M5 line (Fig. 2A and D and Supplementary Material, Fig. S1). Cortical lysates from the M5 mouse line showed a 3.2-fold increase in S935 phosphorylation of endogenous LRRK2 (Fig. 1E).

14-3-3θ Overexpression is protective against G2019S-LRRK2-induced neurite shortening in primary neuronal cultures

Several disease-causing mutations, including the G2019S-LRRK2 mutation, cause a decrease in arborization and overall neurite length in primary hippocampal and cortical cultures (19–23,41). We confirmed total primary neurite shortening in neuronal cultures from a BAC human G2019S-LRRK2 transgenic mouse line that demonstrates the highest level of G2019S-LRRK2 expression in the hippocampus (19,42) (Fig. 2J). To test whether 14-3-3θ overexpression can reverse the effects of the G2019S-LRRK2 mutation on neurite length, we crossed our hemizygous 14-3-3θ overexpressing mice (Fig. 2A–C) with the BAC G2019S-LRRK2 mice and prepared primary hippocampal cultures from pups at postnatal day zero (P0). Primary hippocampal neurons demonstrated cytoplasmic expression of exogenous HA-tagged 14-3-3θ expression, as shown by immunocytochemistry at day *in vitro* (DIV) 8 (Supplementary Material, Fig. S1A). 14-3-3θ overexpression in the BAC G2019S-LRRK2 mouse did not alter LRRK2 transgene expression levels (Fig. 2A and D), yet levels of 14-3-3θ overexpression in primary cultures from double transgenic mice were sufficient to cause an increase in S935 phosphorylation in LRRK2 (Fig. 2D and E). When 14-3-3θ was overexpressed alone, there was no noticeable effect on neurite length compared with nontransgenic cultures (Fig. 2F, G and J). In cultures from double transgenic mice, 14-3-3θ overexpression reversed the neurite shortening due to G2019S-LRRK2 expression (Fig. 2F–J).

14-3-3 Inhibition exacerbates neurite shortening by the G2019S-LRRK2 mutation

We next investigated whether 14-3-3 inhibition would exacerbate neurite shortening induced by G2019S-LRRK2 expression. Neuronal cultures from G2019S-LRRK2 mice were transduced with a tetracycline-inducible lentivirus expressing either difopein-eYFP or mutant difopein-eYFP (control virus) (32), and difopein expression was induced with doxycycline (2 μg/ml) the next day. Difopein expression alone in nontransgenic neurons caused reduced neurite length compared with nontransgenic neurons expressing control mutant difopein (Fig. 3A). Difopein expression in G2019S-LRRK2 neurons additionally decreased total neurite length by 25% compared with G2019S-LRRK2 neurons also expressing the control mutant difopein (Fig. 3A).

We further confirmed these findings by crossing a transgenic mouse expressing difopein-eYFP (40) with the G2019S-LRRK2 mouse. The difopein mouse demonstrated high levels of difopein-eYFP expression in the hippocampus and other brain regions (Fig. 3C-E). Primary hippocampal neurons from difopein-eYFP mice

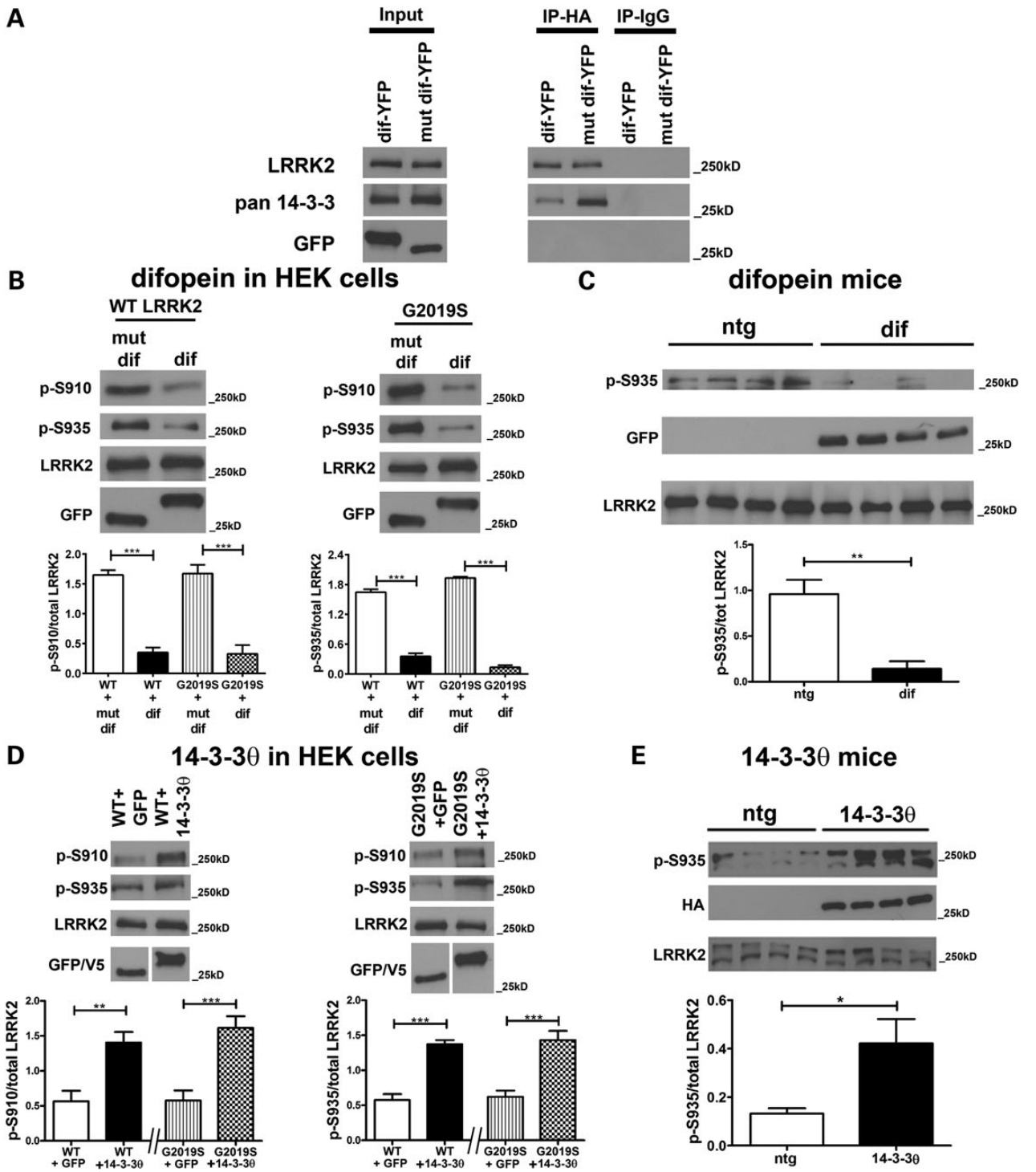

Figure 1. 14-3-3s regulate LRRK2 phosphorylation at serine 910 and 935. (**A**) Western blots from co-immunoprecipitation experiments of endogenous 14-3-3 interaction with HA-tagged LRRK2 protein. Difopein-eYFP migrates slightly higher than mutant difopein-eYFP since difopein has two R18 peptide sequences while the mutant difopein peptide has one copy of the mutated R18 peptide sequence (38). (**B**) Lysates from HEK 293T cells transfected with difopein and either wild type or G2019S-LRRK2 were analyzed for LRRK2 phosphorylation at S910 and S935 and total LRRK2 by western blot. Representative western blots are shown. The ratio of phosphorylated LRRK2 to total LRRK2 is quantified from three independent experiments. ***$P < 0.001$ (unpaired *t*-test). (**C**) Quantification of S935 phosphorylation in hippocampal lysates from wild-type and difopein-eYFP transgenic mice. $n = 4$ mice per group, **$P < 0.01$ (unpaired *t*-test). (**D**) Lysates from HEK 293T cells transfected with GFP or 14-3-3θ and either wild type or G2019S-LRRK2 were analyzed for LRRK2 phosphorylation at S910 and S935 and total LRRK2 by western blot. $n = 3$ independent rounds, **$P < 0.01$, ***$P < 0.001$ (unpaired *t*-test). (**E**) Representative western blots and quantification of S935 phosphorylation in cortical lysates generated from transgenic mice overexpressing 14-3-3θ. $n = 4$ mice per group, *$P < 0.05$ (unpaired *t*-test).

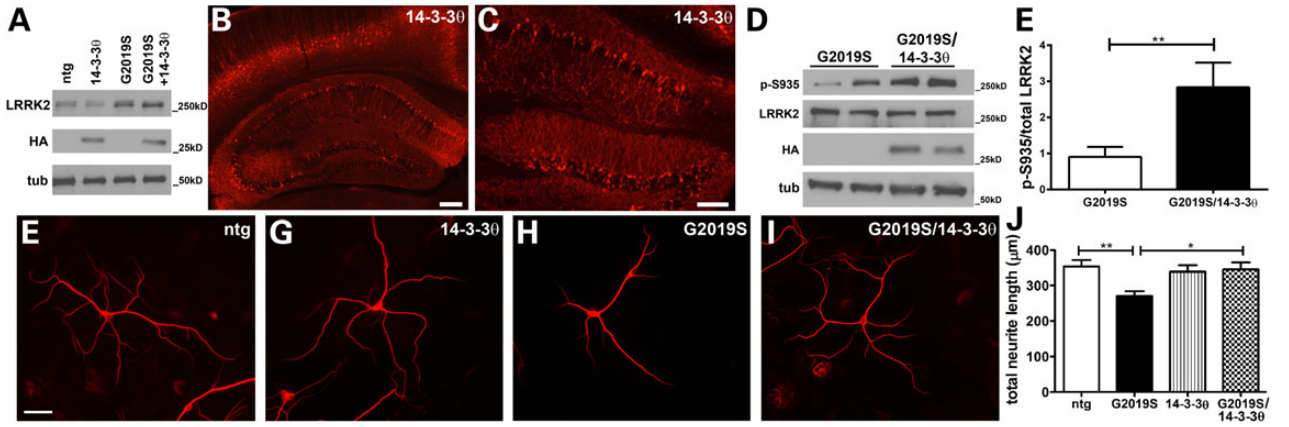

Figure 2. 14-3-3θ overexpression reverses G2019S-LRRK2-mediated neurite shortening in primary hippocampal cultures. (**A**) Western blots against HA-tagged 14-3-3θ and LRRK2 from lysates of dissected hippocampi from 8-day-old transgenic mice. (**B** and **C**) Immunohistochemistry for HA-tagged 14-3-3θ in coronal brain section through the hippocampus from a 14-3-3θ mouse. Scale bar = 200 μm. (**D** and **E**) Western blot of lysates from DIV8 primary hippocampal cultures prepared from nontransgenic (ntg), G2019S-LRRK2, 14-3-3θ and G2019S-LRRK2/14-3-3θ mice to measure S935 LRRK2 phosphorylation. $n = 4$ mice per group, $^{**}P < 0.01$ (unpaired *t*-test). (**F–I**) Representative images of neurons stained for MAP2 from each of the four genotypes represented in the cross. Scale bar = 50 μm. (**J**) Total neurite length analysis of neurons from nontransgenic, G2019S-LRRK2, 14-3-3θ and G2019S-LRRK2/14-3-3θ mouse cultures. $n = 52$ neurons for ntg, $n = 52$ for 14-3-3θ, $n = 65$ for G2019S-LRRK2 and $n = 44$ for G2019S-LRRK2/14-3-3θ combined from three independent rounds. $^{*}P < 0.05$, $^{**}P < 0.01$ (Tukey's multiple comparison test).

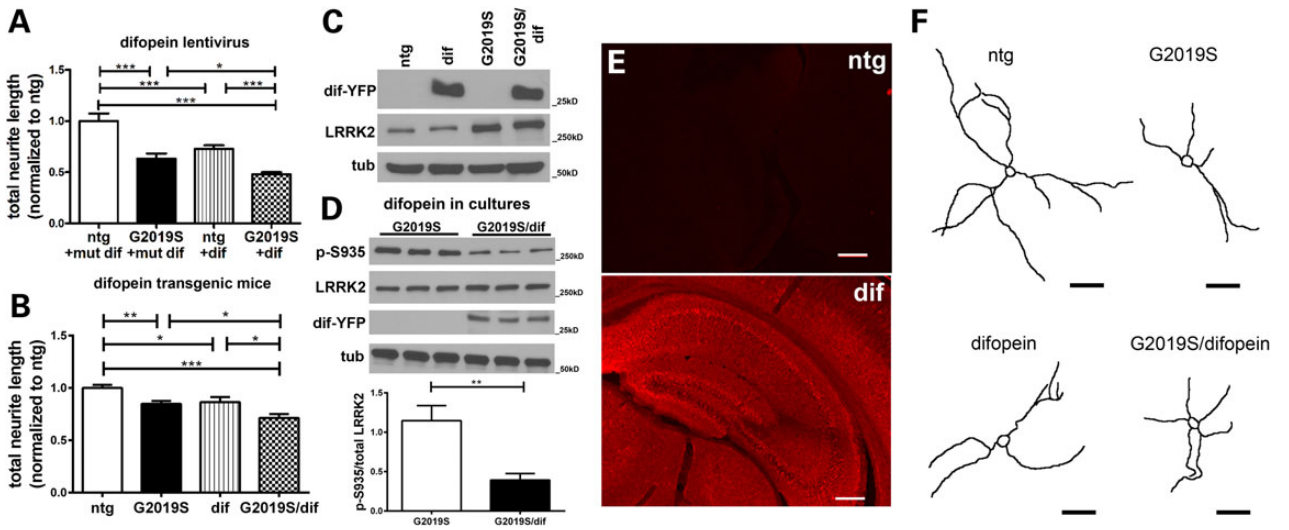

Figure 3. 14-3-3 inhibition with difopein promotes neurite shortening induced by G2019S-LRRK2. (**A**) Primary hippocampal cultures from nontransgenic (ntg) and G2019S-LRRK2 littermates were transduced with a doxycycline-inducible lentivirus expressing either difopein-eYFP (dif) or mutant difopein-eYFP (mut dif) and then treated with doxycycline (2 μg/ml). Total neurite length was measured for neurons expressing eYFP. $n = 22$ neurons for ntg/mut dif, $n = 39$ for ntg/dif, $n = 36$ for G2019S-LRRK2/mut dif and $n = 66$ for G2019S-LRRK2/dif combined from three independent rounds. $^{*}P < 0.05$, $^{***}P < 0.001$ (Tukey's multiple comparison test). (**B**) Total neurite length analysis of neurons from nontransgenic, G2019S-LRRK2, difopein and G2019S-LRRK2/difopein cultures. $n = 34$ neurons for ntg, $n = 17$ for dif, $n = 34$ for G2019S-LRRK2 and $n = 22$ for G2019S-LRRK2/dif combined from three independent rounds. $^{*}P < 0.05$, $^{**}P < 0.01$, $^{***}P < 0.001$ (Tukey's multiple comparison test). (**C**) Western blot for eYFP-tagged difopein and LRRK2 of lysates from dissected hippocampi from 8-day-old transgenic mice. (**D**) Western blot for S935 phosphorylation of lysates from DIV8 primary hippocampal cultures from transgenic mice. $n = 3$ mice per group, $^{**}P < 0.01$ (unpaired t-test). (**E**) Immunohistochemistry for difopein-eYFP in coronal sections through the hippocampus of difopein mice and nontransgenic mice. Scale bar = 500 μm. (**F**) Representative tracings of neurons analyzed in each resulting genotype in the cross. Scale bar = 50 μm.

showed diffuse, cytoplasmic expression of difopein-eYFP, as demonstrated by immunocytochemistry at DIV8 (Supplementary Material, Fig. S1B). LRRK2 transgene expression was unchanged when the BAC G2019S-LRRK2 mouse was crossed with the difopein-eYFP mouse, but S935 phosphorylation of LRRK2 was reduced in cultures from these double transgenic mice (Fig. 3D). Consistent with other experiments (Fig. 3A), neurons from G2019S-LRRK2/difopein double transgenic mice showed a 16% decrease in total neurite length compared with neurons from G2019S-LRRK2 mice (Fig. 3B and F).

Difopein is a pan-14-3-3 inhibitor that binds and inhibits all seven 14-3-3 isoforms. To test whether inhibition of the 14-3-3θ isoform is sufficient to promote G2019S-LRRK2-induced neurite shortening, we tested the effect of a dominant-negative (DN) 14-3-3θ mutant (R56A/R60A) (43) on G2019S-LRRK2-induced neurite shortening. 14-3-3θ forms both homodimers and heterodimers with only a subset of 14-3-3 isoforms (44–47), such that the effects of DN 14-3-3θ is limited to only 14-3-3θ and those isoforms with which it can heterodimerize, allowing the other six isoforms to dimerize with one another. We crossed the

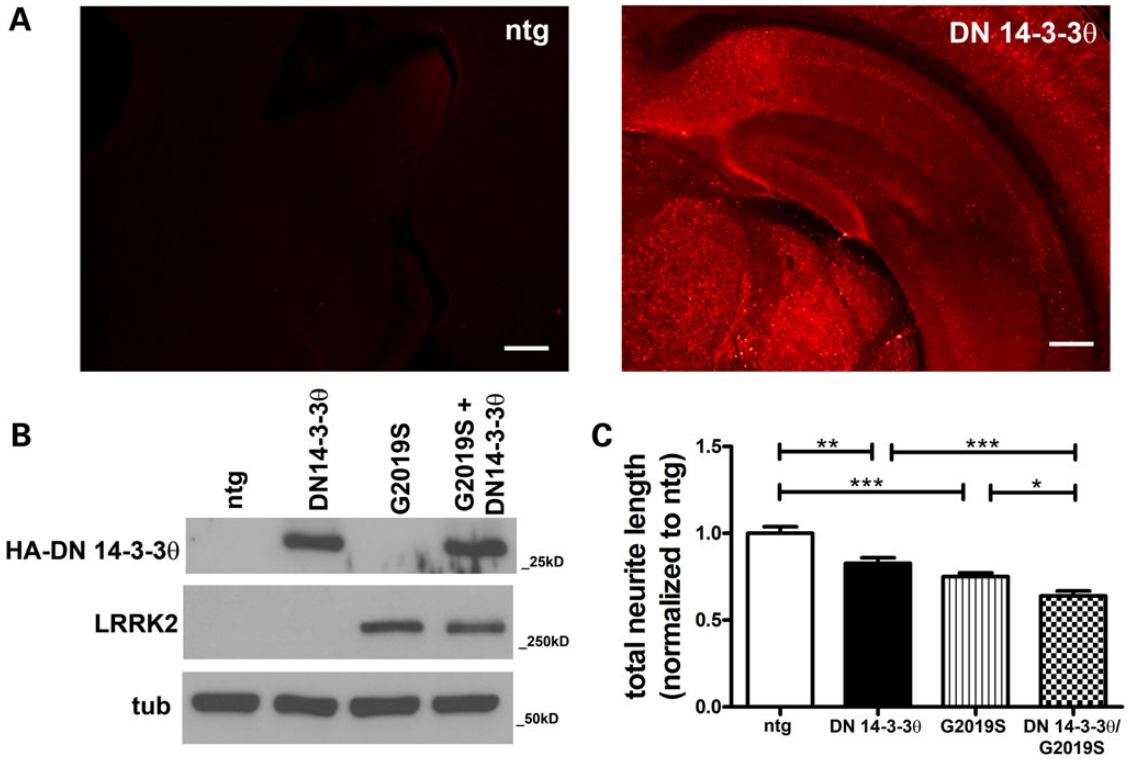

Figure 4. Dominant-negative 14-3-3θ expression also promotes G2019S-LRRK2-induced neurite shortening. (**A**) Immunohistochemistry for HA-tagged DN 14-3-3θ in coronal sections through the hippocampus of DN 14-3-3θ and nontransgenic mice. Scale bar = 500 µm. (**B**) Western blot for HA-tagged 14-3-3θ and LRRK2 from lysates from DIV8 primary hippocampal cultures from transgenic mice. (**C**) Total neurite length analysis of neurons from nontransgenic, G2019S-LRRK2, DN 14-3-3θ and G2019S-LRRK2/DN 14-3-3θ cultures. $n = 25$ neurons for ntg, $n = 50$ for DN 14-3-3θ, $n = 75$ for G2019S-LRRK2 and $n = 35$ for G2019S-LRRK2/DN 14-3-3θ combined from three independent rounds. $^{*}P < 0.05$, $^{**}P < 0.01$, $^{***}P < 0.001$ (Tukey's multiple comparison test).

G2019S-LRRK2 mouse line with a transgenic mouse that overexpresses HA-tagged DN 14-3-3θ under the Thy1.2 promoter. This DN 14-3-3θ mouse showed expression of DN 14-3-3θ in the hippocampus (Fig. 4A), and LRRK2 transgene expression was unchanged in primary cultures from double transgenic mice when the BAC G2019S-LRRK2 mouse was crossed with the DN 14-3-3θ mouse (Fig. 4B). Neurons from G2019S-LRRK2/DN 14-3-3θ double transgenic mice showed a 23% reduction in total neurite length compared with neurons from G2019S-LRRK2 mice (Fig. 4C). Expression of DN 14-3-3θ alone caused a 17.3% reduction in total neurite length compared with that from nontransgenic neurons (Fig. 4C). These data indicated that inhibition of 14-3-3θ is sufficient to cause reduced neurite length, highlighting the importance of this particular isoform.

14-3-3θ overexpression is protective against the R1441G mutation

While G2019S is the most common *LRRK2* mutation found in PD patients, there are several other mutants that cause autosomal-dominant PD, including R1441G-LRRK2. R1441G-LRRK2 has been shown by other groups to have reduced interaction (25,37) or no interaction (26) with 14-3-3s compared with wild type or G2019S-LRRK2. We observed that endogenous 14-3-3s co-immunoprecipitated with myc-tagged R1441G-LRRK2 expressed in HEK293T cells, but at reduced levels when compared with wild-type LRRK2 (Fig. 5A). Similarly, in hippocampal lysates from age-matched BAC wild-type, G2019S, or R1441G-LRRK2 mice, we observed a similar reduction in 14-3-3 co-immunoprecipitation with R1441G-LRRK2 compared with wild type or G2019S-LRRK2, although the interaction was not completely abolished (Fig. 5B). We also observed a reduction in S910 and S935 phosphorylation in R1441G-LRRK2 lysates, which was not reversed by 14-3-3θ overexpression (Fig. 5C).

To test whether 14-3-3θ could reverse neurite shortening by R1441G-LRRK2 despite reduced interaction with R1441G-LRRK2, we crossed our 14-3-3θ transgenic mice with a BAC R1441G-LRRK2 mouse (48). As previously reported (48), we observed that hippocampal neurons from BAC R1441G-LRRK2 mice showed reduced neurite length (Fig. 5D). 14-3-3θ overexpression reversed this neurite shortening by R1441G-LRRK2 (Fig. 5D).

LRRK2-independent effects of 14-3-3 inhibition on neurite growth

Both difopein and DN 14-3-3θ caused neurite shortening not only in cultures from G2019S-LRRK2 mice but also from nontransgenic mice. As hippocampal neurons express endogenous LRRK2 (49,50), we hypothesized that inhibition of 14-3-3s could allow unmasking of endogenous wild-type LRRK2 action on neurite length. To test whether difopein's effect on nontransgenic cultures is dependent upon the presence of endogenous LRRK2, we examined the effect of difopein on neurite length in the LRRK2 null background. Difopein transgenic mice were crossed with LRRK2 heterozygous knockout (+/–) mice, and hippocampal cultures from the resulting mice were analyzed for neurite length. LRRK2 knockout (LRRK2 –/–) cultures showed a mild increase in total neurite length compared with wild-type (LRRK2 +/+) cultures as previously reported (19,20,21), yet difopein caused a similar reduction in neurite length in both wild-type

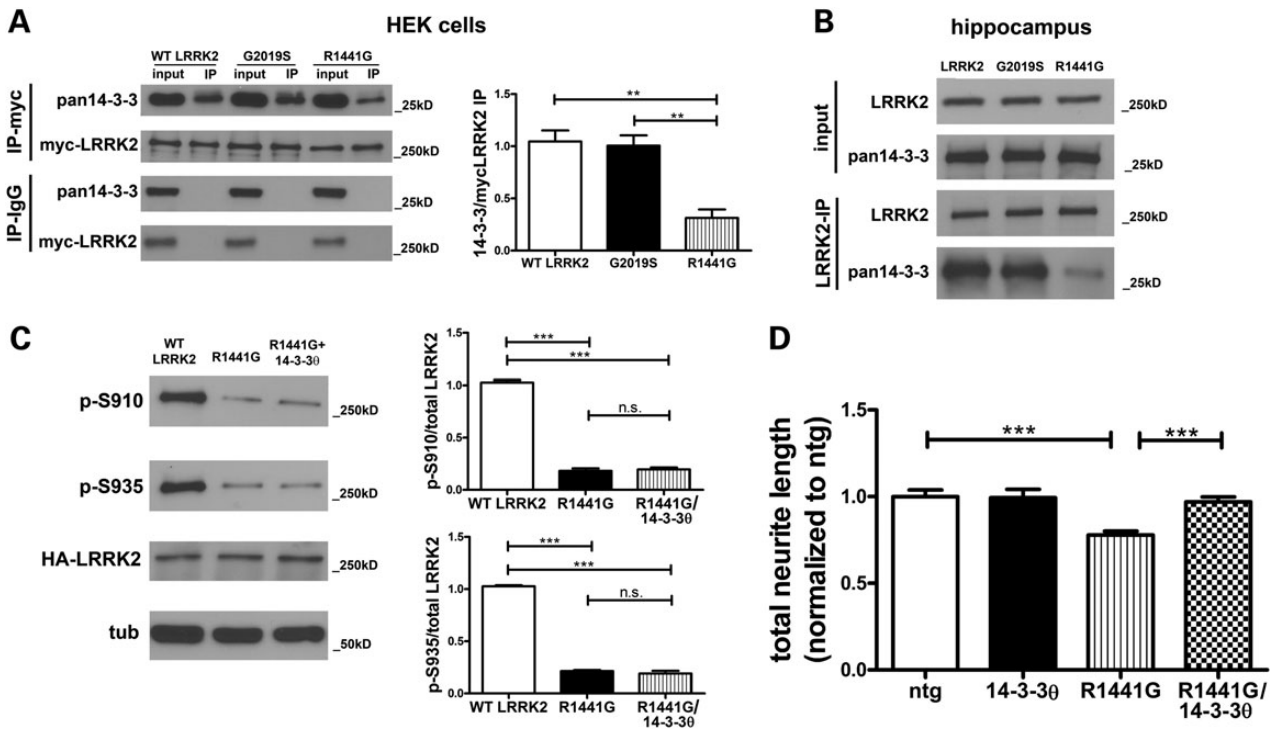

Figure 5. 14-3-3θ overexpression ameliorates R1441G-LRRK2-induced neurite shortening. (**A**) Cell lysates from HEK 293T cells transfected with myc-tagged wild-type, G2019S, or R1441G-LRRK2 were immunoprecipitated with a monoclonal antibody against myc, and resulting immunoprecipitants were analyzed by western blot with a polyclonal rabbit antibody against endogenous 14-3-3s (pan). The ratio of pan 14-3-3 to myc LRRK2 was quantified for three independent rounds. $^{**}P < 0.01$ (Tukey's multiple comparison test). (**B**) Hippocampal lysates from 8-day-old BAC wild-type, G2019S, or R1441G-LRRK2 transgenic mice were immunoprecipitated for LRRK2 and the resulting immunoprecipitates were probed for endogenous 14-3-3s by western blot. (**C**) Lysates from HEK 293T cells transfected with V5-tagged 14-3-3θ and either wild type or R1441G-LRRK2 were analyzed for LRRK2 phosphorylation at S910 and S935 and total LRRK2 by western blot. The ratio of phosphorylated LRRK2 to total LRRK2 was quantified for three independent rounds. $^{***}P < 0.001$, ns = not significant (Tukey's multiple comparison test). (**D**) Total neurite length analysis of neurons from nontransgenic, R1441G-LRRK2, 14-3-3θ and R1441G-LRRK2/DN 14-3-3θ cultures. $n = 29$ neurons for ntg, $n = 22$ for 14-3-3θ, $n = 48$ for R1441G-LRRK2 and $n = 55$ for R1441G-LRRK2/14-3-3θ combined from three independent rounds. $^{***}P < 0.001$ (Tukey's multiple comparison test).

(LRRK2 +/+) and LRRK2 –/– cultures (Fig. 6A). This finding suggests that difopein can reduce neurite length through a LRRK2-independent mechanism.

To test whether DN 14-3-3θ's effect on neurites was dependent on endogenous LRRK2, we crossed DN 14-3-3θ mice with LRRK2 +/– mice. DN 14-3-3θ expression caused a reduction in neurite length, even in the absence of LRRK2 (Fig. 6B).

14-3-3θ regulates LRRK2 kinase activity

The G2019S-LRRK2 mutation is thought to confer toxicity through an increase in its kinase activity (11–15,51), and neurite shortening has been shown to be kinase-dependent (15,19,20). To test whether 14-3-3θ protects against G2019S-LRRK2 neurotoxicity by reducing its kinase activity, we examined the effect of 14-3-3θ on both wild-type and G2019S-LRRK2 kinase activity. HEK293T cells were transfected with HA-tagged wild type or G2019S-LRRK2 with or without 14-3-3θ, and then immunoprecipitated for HA-tagged LRRK2 using a monoclonal antibody against HA prior to performing the kinase assay. Kinase activity was measured by the level of autophosphorylation at threonine 1503 (T1503) in LRRK2 (52). We measured a 1.7-fold increase in T1503 phosphorylation with the G2019S-LRRK2 when compared with wild-type LRRK2 (Fig. 7A). When 14-3-3θ was co-transfected with G2019S-LRRK2, T1503 phosphorylation decreased by 50%. The effect of 14-3-3θ on G2019S-LRRK2 was dose-dependent, with a greater reduction of T1503 phosphorylation with increasing amounts of 14-3-3θ expression (Fig. 7A).

We next tested the effects of 14-3-3 inhibition on LRRK2 kinase activity in HEK293T cells. HEK293T cells co-transfected with difopein and wild-type LRRK2 showed a 2.4-fold increase in kinase activity compared with cells transfected with wild-type LRRK2 and mutant difopein (Fig. 7B). G2019S-LRRK2 showed a 2.2-fold increase in kinase activity compared with wild-type LRRK2, and in the presence of difopein, G2019S-LRRK2 kinase activity was increased by 74% (Fig. 7B).

As another measure of LRRK2 kinase activity, we examined LRRK2 phosphorylation at S1292. LRRK2 autophosphorylation at the S1292 site correlates with LRRK2 kinase activity (15). S1292 phosphorylation was increased by 1.7-fold in HEK293T cells transfected with G2019S-LRRK2 compared with cells transfected with wild-type LRRK2 (Fig. 7C). When 14-3-3θ was cotransfected with G2019S-LRRK2, S1292 phosphorylation was reduced by 46% (Fig. 7C). The effect of 14-3-3θ on LRRK2 was dose-dependent, with a greater reduction of S1292 phosphorylation with increasing amounts of 14-3-3θ expression with G2019S-LRRK2 (Fig. 7C). Conversely, S1292 phosphorylation increased by 62% when G2019S-LRRK2 was transfected together with constructs expressing difopein (Fig. 7D). Difopein also increased S1292 phosphorylation 3.5-fold when co-transfected with wild-type LRRK2 (Fig. 7D).

Next, we measured S1292 phosphorylation in lysates from microdissected hippocampi from 6-week-old mice. G2019S-LRRK2/14-3-3θ double transgenic mice showed a 79% decrease in S1292 phosphorylation compared with G2019S-LRRK2 littermates (Fig. 7E). In contrast, G2019S-LRRK2/difopein mice showed

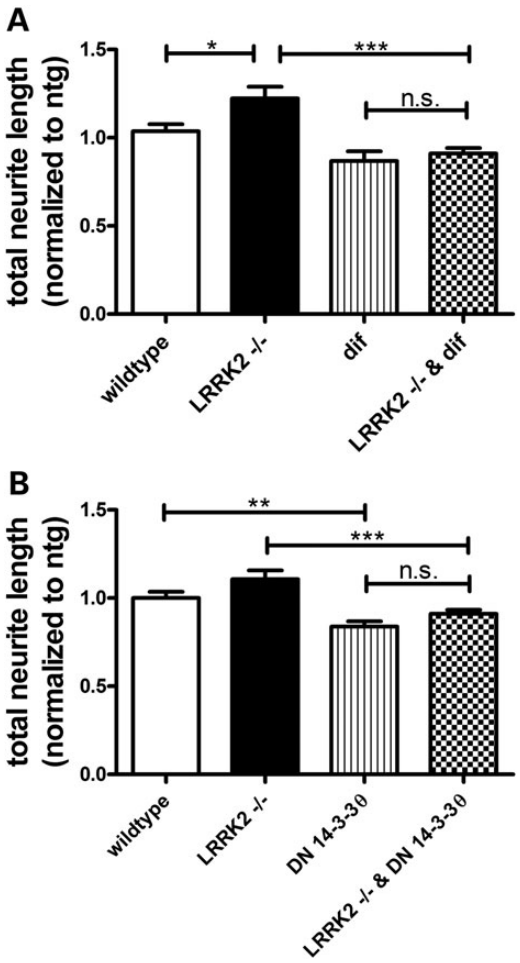

Figure 6. Difopein and DN 14-3-3θ cause neurite shortening in the absence of LRRK2 expression. (**A**) Total neurite length analysis of neurons from difopein-eYFP crossed with LRRK2 –/– cultures. $n = 22$ neurons for wild type (wt), $n = 16$ for LRRK2 –/–, $n = 16$ for dif and $n = 22$ for LRRK2 –/– + dif combined from four independent rounds. *$P < 0.05$, ***$P < 0.001$, ns = nonsignificant (Tukey's multiple comparison test). (**B**) Total neurite length analysis of neurons from DN 14-3-3θ crossed with LRRK2 –/– cultures. $n = 23$ neurons for wt, $n = 25$ for LRRK2 –/–, $n = 44$ for DN 14-3-3θ and $n = 39$ for LRRK2 –/– + DN 14-3-3θ combined from four independent rounds. **$P < 0.01$, ***$P < 0.001$, ns = nonsignificant (Tukey's multiple comparison test).

a 2.3-fold increase in hippocampal S1292 phosphorylation compared with G2019S-LRRK2 mice (Fig. 7F).

Finally, we measured the effect of 14-3-3θ overexpression on the phosphorylation of a known *in vitro* substrate of LRRK2, ADP-ribosylation factor GTPase-activating protein 1 (ArfGAP1) (53,54). Lysates from HEK293T cells transfected with LRRK2 with and without 14-3-3θ were immunoprecipitated for HA-tagged wild type or G2019S-LRRK2, and then recombinant ArfGAP1 was added to the immunoprecipitate prior to the kinase reaction. As expected, G2019S-LRRK2 caused a 2-fold increase in ArfGAP1 phosphorylation compared with wild-type LRRK2 (Fig. 7G). Co-transfection of 14-3-3θ with G2019S-LRRK2 decreased ArfGAP1 phosphorylation to wild-type LRRK2 levels, while 14-3-3θ co-expression with wild-type LRRK2 did not affect ArfGAP1 phosphorylation (Fig. 7G).

14-3-3θ Binds LRRK2 directly to regulate kinase activity

To determine whether a direct interaction between 14-3-3θ and LRRK2 is required in order for 14-3-3θ to regulate LRRK2 kinase activity, we tested the ability of 14-3-3θ to regulate the kinase activity of LRRK2 mutants that cannot bind 14-3-3s. As previously shown (24–26), the S935A mutation of LRRK2 eliminates the ability of 14-3-3s to bind LRRK2, which we confirmed by immunoprecipitation (Fig. 8). Phosphorylation at T1503 was similar with the S935A mutant compared with wild-type LRRK2. Likewise, the S935A mutation did not alter phosphorylation at T1503 in G2019S-LRRK2 (Fig. 8). While 14-3-3θ overexpression reduced T1503 phosphorylation of wild type and G2019S-LRRK2, it did not reduce T1503 phosphorylation in the presence of the S935A mutation in either wild type or G2019S-LRRK2 (Fig. 8). These results suggest that 14-3-3θ must directly interact with LRRK2 in order to regulate LRRK2 kinase activity.

LRRK2 kinase inhibitors reverse-enhanced neurite shortening in G2019S-LRRK2/difopein double transgenic cultures

If the effect of 14-3-3s on G2019S-LRRK2 toxicity were mediated by the ability of 14-3-3s to regulate LRRK2 kinase activity, we predicted that the exacerbation of G2910S-LRRK2-induced neurite retraction by difopein would be reversed by LRRK2 kinase inhibitors. Primary cultures from G2019S-LRRK2/difopein double transgenic mice were treated with the LRRK2 kinase inhibitor, HG-10-102-01 (55) at 1.5 μM at DIV6, and cultures were then fixed and stained for neurite analysis at DIV8. HG-10-102-01 caused a reversal of neurite shortening in G2019S-LRRK2/difopein primary neuron cultures (Fig. 9A). HG-10-102-01 did not alter neurite length in LRRK2 –/– cultures, suggesting that HG-10-102-01 effects on neurite length were caused by LRRK2 inhibition (Supplementary Material, Fig. S2). These findings suggest that the exacerbation of neurite shortening in G2019S-LRRK2/difopein cultures is mediated in part through increased LRRK2 kinase activity.

We next tested the effects of HG-10-102-01 treatment in primary cultures from G2019S-LRRK2/14-3-3θ double transgenic mice. Untreated G2019S-LRRK2/14-3-3θ neurons showed neurite lengths comparable with nontransgenic neurons (Fig. 9B). In cultures from G2019S-LRRK2/14-3-3θ mice, the addition of HG-10-102-01 caused further increase in neurite length compared with control G2019S-LRRK2/14-3-3θ neurons (Fig. 9B). These findings suggest that 14-3-3θ overexpression and LRRK2 inhibitors may act synergistically to promote neurite length.

Discussion

In this study, we demonstrate that 14-3-3s can regulate several aspects of LRRK2 biology, including phosphorylation, kinase activity and regulation of neurite length. 14-3-3θ overexpression increased LRRK2 phosphorylation at S910 and S935 in both wild type and G2019S-LRRK2, while 14-3-3 inhibition by difopein reduced S910 and S935 phosphorylation. 14-3-3θ overexpression also reversed neurite shortening induced by G2019S or R1441G-LRRK2 mutations, while inhibition of all 14-3-3 isoforms promoted further neurite shortening. 14-3-3θ inhibition with the dominant-negative 14-3-3θ similarly enhanced neurite shortening by G2019S-LRRK2, suggesting that inhibition of the 14-3-3θ isoform is sufficient to affect mutant LRRK2-mediated neurite shortening. The effect of 14-3-3θ expression on LRRK2 function is likely mediated through effects on LRRK2 kinase activity. 14-3-3θ Overexpression reduced G2019S-LRRK2 kinase activity both *in vitro* and *in vivo*, as measured by autophosphorylation and phosphorylation of a known *in vitro* LRRK2 substrate, ArfGAP1. Notably, 14-3-3θ's effect on kinase activity was dose-dependent.

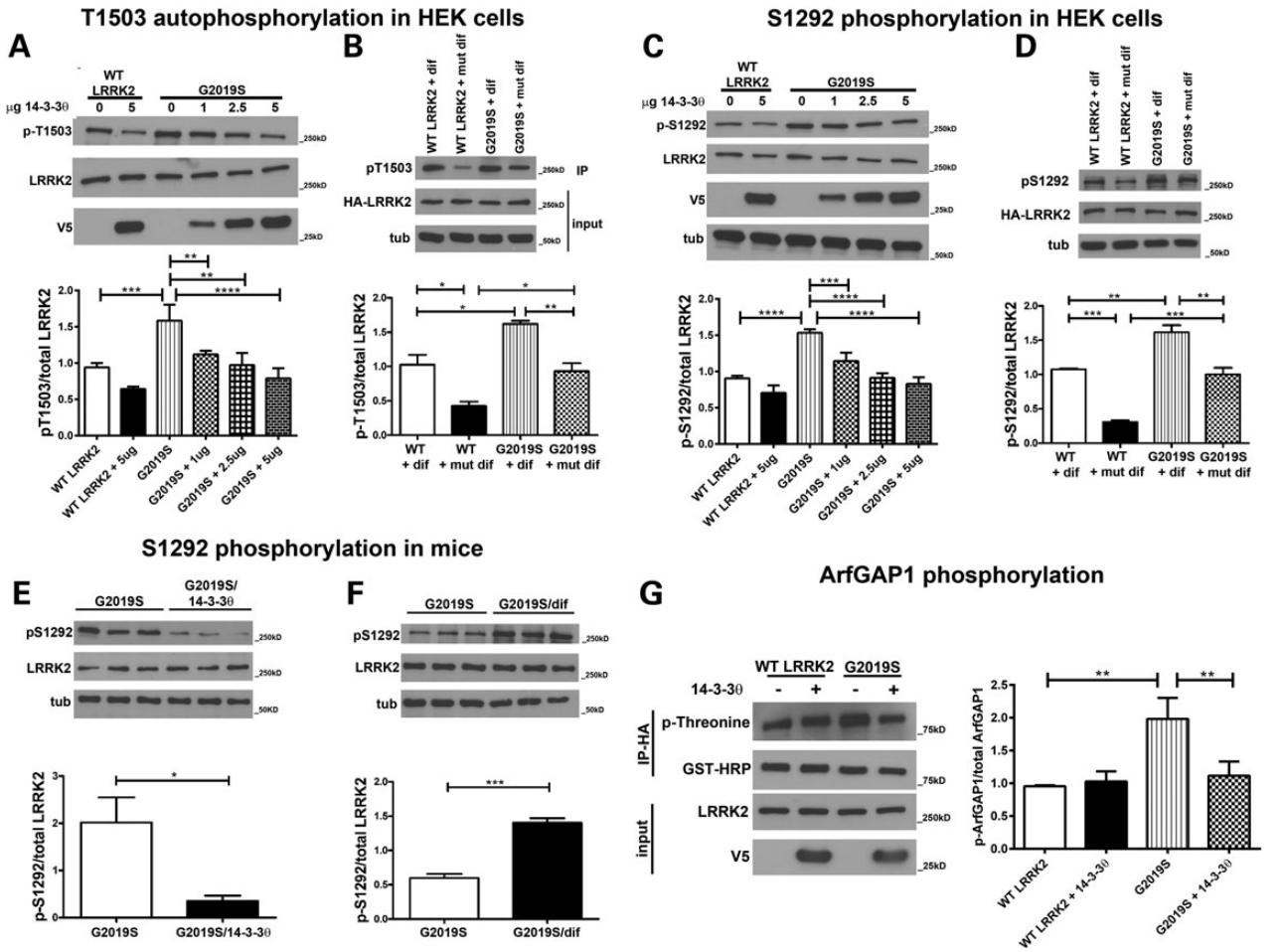

Figure 7. 14-3-3s regulates LRRK2 autophosphorylation and *trans*-phosphorylation activities. (**A**) Lysates from HEK293T cells transfected with wt or G2019S-LRRK2 together with increasing amounts of V5-tagged 14-3-3θ plasmid were generated. LRRK2 was immunoprecipitated with a HA-specific antibody to isolate LRRK2 for *in vitro* kinase reactions. Following kinase reaction, immunoprecipitates were then analyzed for the LRRK2 autophosphorylation residue phospho-T1503 and total HA-tagged LRRK2 by western blot. $n = 3$ independent rounds. $^{**}P < 0.01$, $^{***}P < 0.001$, $^{****}P < 0.0001$ (Tukey's multiple comparison test). (**B**) Lysates from HEK293T cells transfected with wt or G2019S-LRRK2 together with difopein-eYFP or mutant difopein-eYFP were immunoprecipitated with a HA-specific antibody prior to the kinase assay. After the kinase reaction, immunoprecipitates were probed for phospho-T1503 and total HA-tagged LRRK2 by western blot. $n = 3$ independent rounds. $^{*}P < 0.05$, $^{**}P < 0.01$ (Tukey's multiple comparison test). (**C**) Lysates from HEK 293T cells transfected with wt or G2019S-LRRK2 along with increasing amounts of V5-tagged 14-3-3θ plasmid were analyzed for LRRK2 autophosphorylation at S1292 and total LRRK2 by western blot. $n = 4$ independent rounds. $^{***}P < 0.001$, $^{****}P < 0.0001$ (Tukey's multiple comparison test). (**D**) Lysates from HEK 293T cells transfected with wt or G2019S-LRRK2 along with difopein-eYFP or mutant difopein-eYFP were analyzed for LRRK2 autophosphorylation at S1292 and total LRRK2 by western blot. $n = 3$ independent rounds. $^{**}P < 0.01$, $^{***}P < 0.001$ (Tukey's multiple comparison test). (**E**) Hippocampal lysates from 6-week-old G2019S-LRRK2 or G2019S-LRRK2/14-3-3θ littermates were analyzed for LRRK2 autophosphorylation at S1292 and total LRRK2 by western blot. $n = 3$ mice per group, $^{*}P < 0.05$ (unpaired *t*-test). (**F**) Hippocampal lysates from 6-week-old G2019S-LRRK2 or G2019S-LRRK2/difopein-eYFP littermates were analyzed for LRRK2 autophosphorylation at S1292 and total LRRK2 by western blot. $n = 3$ mice per group, $^{***}P < 0.001$ (unpaired *t*-test). (**G**) Lysates from HEK293T cells transfected with wt or G2019S-LRRK2 with and without V5-tagged 14-3-3θ were immunoprecipitated with an HA-specific antibody prior to performing the kinase assay. Kinase assays were performed with immunoprecipitates together with recombinant GST-tagged ArfGAP1. Following incubation in kinase buffer, immunoprecipitates were then probed for phospho-threonine and GST by western blot. $n = 3$ independent rounds. $^{**}P < 0.01$ (Tukey's multiple comparison test).

Conversely, difopein expression increased LRRK2 kinase activity *in vitro* and *in vivo*. The ability of 14-3-3θ to reduce LRRK2 kinase activity was dependent on direct binding of 14-3-3θ to LRRK2, as 14-3-3θ had no effect on the kinase activity of the non-14-3-3 binding S935A-LRRK2 mutant. Finally, treatment of primary cultures from G2019S-LRRK2/difopein double transgenic mice with a selective LRRK2 kinase inhibitor HG-10-102-01 reversed the enhanced neurite shortening observed in these double transgenic cultures.

The interaction between 14-3-3s and LRRK2 is well established, but the biological significance of this interaction with regards to LRRK2 kinase activity and function is not clear (25,26,37). Our findings demonstrate that 14-3-3s can regulate LRRK2 kinase activity and function so that alterations in 14-3-3 binding to LRRK2 may be important in LRRK2-linked disease. Several LRRK2 mutants show reduced binding to 14-3-3s (25,26,37) that could lead to increased LRRK2 kinase activity and thereby toxicity. This increase in LRRK2 kinase activity would not necessarily be apparent in kinase assays using recombinant LRRK2 fragments that lack the ability to interact with 14-3-3s. In addition, reduced 14-3-3 expression and function has been demonstrated in PD models and human PD (30–32,34) and could potentially lead to increased LRRK2 kinase activity that could contribute to the neurodegenerative process.

We have previously evaluated the effects of 14-3-3s in several other PD model systems. Overexpression of 14-3-3θ reduces toxicity of both rotenone and 1-methyl-4-phenylpyridinium (MPP^+)

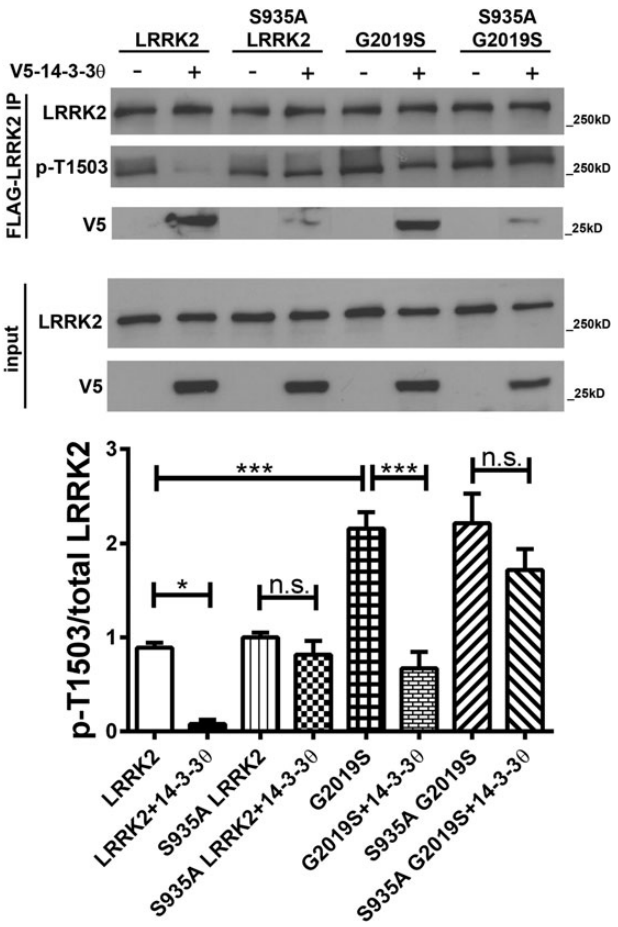

Figure 8. Binding to LRRK2 is required for 14-3-3θ regulation of LRRK2 kinase activity. HEK 293T cells were cotransfected with either FLAG-tagged wt or G2019S-LRRK2 with and without the S935A mutation and V5-tagged 14-3-3θ. Lysates were immunoprecipitated with FLAG antibodies. Kinase assays were performed with immunoprecipitates. Resultant immunoprecipitants were analyzed by western blot for phospho-T1503, and for LRRK2 and V5 to verify that 14-3-3 co-immunoprecipitation was disrupted by the S935A mutation. $n = 4$ independent rounds. $^{*}P < 0.05$, $^{***}P < 0.001$, n.s. = not significant (Tukey's multiple comparison test).

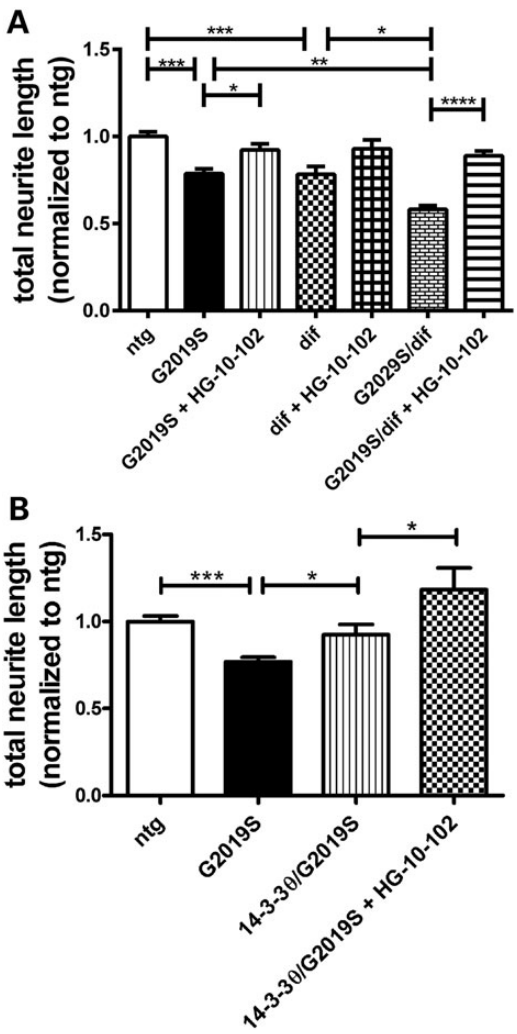

Figure 9. The LRRK2 kinase inhibitor HG-10-102-01 reverses the enhanced neurite shortening observed in the G2019S-LRRK2/difopein double transgenic mice. (**A**) Total neurite length analysis of primary hippocampal neurons from nontransgenic, G2019S-LRRK2, difopein-eYFP and G2019S-LRRK2/difopein-eYFP mouse cultures treated with HG-10-102-01 (1 μM) for 48 h prior to fixing and staining. $n = 45$ neurons for ntg, $n = 21$ for G2019S-LRRK2, $n = 25$ for G2019S-LRRK2 + HG-10-102, $n = 24$ for dif and $n = 21$ for dif + HG-10-102, $n = 23$ for G2019S-LRRK2/dif, $n = 24$ for G2019S-LRRK2/dif + HG-10-102 combined from four independent rounds. $^{*}P < 0.05$, $^{**}P < 0.01$, $^{***}P < 0.001$, $^{****}P < 0.0001$ (Tukey's multiple comparison test). (**B**) Total neurite length analysis of neurons from nontransgenic, G2019S-LRRK2, 14-3-3θ and G2019S-LRRK2/14-3-3θ mouse cultures treated with HG-10-102-01 (1 μM) for 48 h prior to fixing and staining. $n = 27$ neurons for ntg, $n = 44$ for G2019S-LRRK2 and $n = 20$ for G2019S-LRRK2/14-3-3θ, $n = 11$ for G2019S-LRRK2/14-3-3θ + HG-10-102 combined from three independent rounds. $^{*}P < 0.05$, $^{***}P < 0.001$ (Tukey's multiple comparison test).

in vitro, reduces dopaminergic cell loss in an invertebrate αsyn model, and promotes earlier striatal dopamine metabolite recovery in MPTP-treated mice (32,35,36). Our data expand the evidence for the neuroprotective effects of 14-3-3s in PD into pathways relevant to late-onset PD and suggest that 14-3-3s may serve as a therapeutic target for intervention in both idiopathic and genetic forms of disease. Indeed, several commercially available drugs induce 14-3-3 expression at both the mRNA and protein levels—suggesting the potential of small molecule treatments to enhance 14-3-3 expression (56–60).

We observed that 14-3-3s potently regulate LRRK2 phosphorylation at S910 and S935, consistent with other studies using different approaches (25,26,37). These phosphorylation sites have been shown to be dephosphorylated by PP1 (39). Here, we show that difopein, which disrupts the 14-3-3/LRRK2 interaction, caused reduced S910 and S935 phosphorylation of LRRK2 while 14-3-3θ increased S910 and S935 phosphorylation. These data suggest that 14-3-3 binding protects these LRRK2 phosphorylation sites from dephosphorylation. Indeed, this is consistent with the finding by Lobbestael *et al.* (39), who observed that PP1 inhibition with calyculin A was associated with restoration of 14-3-3 binding by LRRK2 under conditions that disrupt the 14-3-3/LRRK2 interaction. Alternatively, 14-3-3 binding could expose S910 and S935 to kinases that phosphorylate LRRK2, including protein kinase A and IκB kinase (25,61,62).

In our study, we demonstrated that 14-3-3θ overexpression can reduce the neurite shortening effects associated with both G2019S and R1441G-LRRK2 expression. G2019S-LRRK2 interacts with 14-3-3s, as we and others (24–26) have observed. R1441G-LRRK2 either does not bind endogenous 14-3-3s (26,37) or shows dramatically reduced interaction with 14-3-3s depending on the experimental parameters (25,39). Here, we did detect endogenous 14-3-3 interaction with R1441G-LRRK2, although at

reduced levels compared with that of wild type or G2019S-LRRK2 (Fig. 5A–C). Our data are consistent with a model in which 14-3-3s directly interact with mutant LRRK2 to reduce kinase activity.

It is possible that there may be intermediary steps required for 14-3-3θ to regulate LRRK2 kinase activity, especially in the case of R1441G-LRRK2 which has reduced binding to 14-3-3s. To determine whether direct interaction between 14-3-3θ and LRRK2 is required for the ability of 14-3-3θ to regulate LRRK2 kinase activity, we evaluated the effect of 14-3-3θ overexpression on the S935A-LRRK2 mutant which cannot bind 14-3-3s. 14-3-3θ Was unable to reduce kinase activity of wild type or G2019S-LRRK2 when mutated at S935 to disrupt the interaction with 14-3-3s. Thus, we conclude that 14-3-3θ acts to inhibit kinase activity by direct binding to LRRK2.

There are several possible ways 14-3-3s may regulate LRRK2 kinase activity. 14-3-3s Normally act as dimers to bind enzymes and cause conformational changes to alter activity. 14-3-3s Have been shown to affect several kinases through these direct interactions (29,63). Our data with the S935A-LRRK2 mutant suggest that 14-3-3θ does need to directly bind to LRRK2 to regulate LRRK2 kinase activity. One possibility is that 14-3-3θ binding could stabilize wild type and G2019S-LRRK2 into a kinase inactive conformation. 14-3-3θ Overexpression could allow for more 14-3-3θ to bind LRRK2 to hold it in an inactive state, while disruption of 14-3-3 binding could promote the formation of active-state LRRK2.

An interesting finding in our study was that difopein caused neurite shortening in nontransgenic cultures. 14-3-3 Proteins have been shown to regulate both axonal and dendritic growth through several mechanisms, including regulation of the cell adhesion molecules L1 and neural cell adhesion molecule, actin depolymerizing factor, neuron navigator 2 and SLIT and NTRK-like family member 1 (64–68). 14-3-3s have also been implicated in protecting phosphorylation sites on Raf1 and MEK, leading to persistent activation of the MEK–ERK pathway which plays a role in neurite outgrowth as well (69–72). Interestingly, different isoforms cause differential effects on neurite length, with some promoting extension and others causing retraction. In our study, we observed that inhibition of all 14-3-3s with difopein caused shortened neurites, suggesting that the sum effect of all endogenous 14-3-3s is to promote elongation.

As difopein's effect on neurite outgrowth occurs in wild-type and LRRK2 knockout cultures in a similar manner, it is reasonable to conclude that 14-3-3s affect neurite outgrowth through LRRK2-independent mechanisms. However, these results do not preclude the possibility of 14-3-3s regulating LRRK2 effects on neurite growth. Indeed, our kinase assay data and our LRRK2 kinase inhibition studies suggest that difopein's exacerbation of effects on G2019S-LRRK2-mediated neurite shortening is likely secondary to difopein upregulating LRRK2 kinase activity. Our kinase assay studies demonstrated that difopein increases G2019S-LRRK2 kinase activity, both with respect to autophosphorylation and *trans*-phosphorylation of a LRRK2 kinase substrate ArfGAP1. G2019S-LRRK2's effect on neurite length is kinase-dependent, as LRRK2 kinase inhibitors can reverse neurite shortening caused by G2019S-LRRK2 expression (15). Finally, the specific LRRK2 kinase inhibitor HG-10-102-01 reverses difopein's exacerbation of neurite shortening of G2019S-LRRK2 neurons. 14-3-3's effects on neurite growth are complex and involve several mechanisms, and in the presence of mutant LRRK2, 14-3-3s can regulate mutant LRRK2-mediated neurite effects through regulation of kinase activity.

If 14-3-3θ acts to restore neurite length in G2019S-LRRK2 cultures by inhibiting LRRK2 kinase activity, we would predict that additional LRRK2 kinase inhibition should not have any additional effect on neurite length in the presence of 14-3-3θ overexpression. However, the addition of LRRK2 kinase inhibitor showed a synergistic effect on neurite length in 14-3-3θ/G2019S-LRRK2 cultures. One possibility is that the amount of 14-3-3θ overexpression in our cultures does not fully inhibit all LRRK2 kinase activity. Indeed, our *in vitro* kinase assays show that 14-3-3θ did not fully eliminate G2019S-LRRK2 kinase activity. The addition of the LRRK2 inhibitor may cause neurite elongation by fully inhibiting any remaining active LRRK2 within the cell.

In conclusion, our studies reveal that 14-3-3s can regulate mutant LRRK2 kinase activity and action on neurite outgrowth. 14-3-3θ overexpression reduces mutant LRRK2 neurite effects by inhibition of kinase activity, while 14-3-3 inhibition enhances LRRK2 kinase activity and neurite shortening. Therefore, increasing the expression of 14-3-3 proteins may provide a new therapeutic avenue to addressing PD caused by LRRK2 mutations.

Material and Methods

Cell transfection

HEK 293T cells were grown in DMEM containing 10% normal calf serum with 1% penicillin/streptomycin. Twenty-four hours after plating, cells were transfected using Superfect transfection reagent (Qiagen, Germantown, MD) using manufacturer's guidelines. After transfection, cells were incubated in fresh media for 48 h prior to protein collection.

Immunoblotting

HEK 293T cells or primary cultured neurons were washed in phosphate buffered saline (PBS) and pelleted at 1500*g* for five minutes. Cell pellets were then sonicated in lysis buffer [150 mM NaCl, 10 mM Tris–HCl pH 7.4, 1 mM EGTA, 1 mM EDTA, 0.5% NP-40, protease inhibitor cocktail and phosphatase inhibitor cocktail (Roche Diagnostics, Indianapolis, IN)], followed by centrifugation at 16 000*g* for 10 min. Protein concentrations were assessed by BCA assay (Pierce, Rockford, IL). Samples were boiled for five minutes in DTT sample loading buffer (0.25 M Tris–HCl pH 6.8, 8% SDS, 200 mM DTT, 30% glycerol, bromophenol blue), resolved on 7.5 or 12% SDS-polyacrylamide gels, and transferred to nitrocellulose membranes. After blocking in 5% nonfat dry milk in TBST (25 mM Tris–HCl pH 7.6, 137 mM NaCl, 0.1% Tween 20), membranes were incubated overnight in rabbit polyclonal antibody against pan-14-3-3 (1:1000 Abcam, Cambridge, MA), rabbit polyclonal antibody against GFP (1:5000 Abcam), mouse monoclonal antibody against HA (1:1000 Covance, Princeton, NJ), mouse monoclonal antibody against FLAG (1:1000 Sigma, St. Louis, MO), rabbit polyclonal antibody against LRRK2 (1:1000 Abcam), rabbit polyclonal antibody against alpha-tubulin (1:2500 Cell Signaling, Danvers, MA), rabbit polyclonal antibody against phosphorylated T1503 LRRK2 (1:1000 Abcam) or rabbit polyclonal antibody against phosphorylated S1292 LRRK2 (1:1000 Abcam) at 4°C. Membranes were then incubated in HRP-conjugated goat anti-mouse or anti-rabbit secondary antibody (1:2000 Jackson ImmunoResearch Laboratories, West Grove, PA) for 2 hours and then washed in TBST six times for 10 min each. Blots were developed with the enhanced chemiluminescence method (GE Healthcare, Piscataway, NJ). Images were scanned and analyzed using Un-ScanIT software (Orem, UT) for densitometric analysis of bands.

Hippocampi and cortices from mouse brains were homogenized in lysis buffer (Tris/HCl 50 mM pH 7.4, NaCl 175 mM, EDTA

5 mM, protease inhibitor and phosphatase inhibitor cocktails) and sonicated for 10 s. Cell lysates were then incubated on ice for 30 min after the addition of 1% Triton X-100 and then spun at 15 000*g* for 1 h at 4°C. The supernatant was saved as the Triton X-100 soluble fraction. Samples were resolved on SDS-polyacrylamide gels and analyzed by western blotting as described above.

Immunoprecipitation

For immunoprecipitation of HA-tagged LRRK2, Protein G Dynabeads (Life Technologies, Grand Island, NY) were incubated with 4 µg mouse HA antibody (Sigma) overnight. Of note, 500 µg of cell lysate was incubated with antibody-conjugated beads for 30 min at room temperature. Beads were then washed five times in PBS with 0.02% Tween. After washing, beads were boiled in DTT sample loading buffer and loaded on a SDS-polyacrylamide gel. After transfer to nitrocellulose, the membrane was probed for 14-3-3 proteins using a polyclonal rabbit antibody against 14-3-3s (1:1000 Abcam). For immunoprecipitation of FLAG-tagged LRRK2, immunoprecipitation was performed using anti-FLAG affinity gel (Sigma) following the manufacturer's protocol.

LRRK2 kinase assay

HEK 293 T cells were transfected with HA-tagged LRRK2 with or without V5-tagged 14-3-3θ or difopein-YFP. Forty-eight hours after transfection, cell lysates were incubated with HA-antibody-conjugated Dynabeads for 30 min. Beads were washed with PBS with two high salt washes of PBS with 500 mM NaCl before being resuspended in kinase buffer (10 mM Tris pH 7.4, 0.1 mM EGTA, 20 mM $MgCl_2$, 0.1 mM ATP). The samples were then shaken at 30°C for 30 min. The kinase reaction was terminated by incubating samples on ice and beads were then incubated in Laemmli buffer at 75°C for 10 min. Sample was then run on a 7.5% SDS-acrylamide gel, transferred to nitrocellulose, and probed for phosphorylated LRRK2 at T1503 using a primary rabbit antibody against phospho-T1503 (1:1000, Abcam) and for total LRRK2 using an antibody against the HA tag (1:1000, Covance).

For measuring LRRK2 kinase activity via ArfGAP1 phosphorylation, the same kinase assay protocol was followed, but 1 µg recombinant ArfGAP1 (Abnova, Taipei City, Taiwan) was added to the kinase buffer prior to the 30 min incubation at 30°C. Samples were electrophoresed on 7.5% SDS-acrylamide gel, transferred to nitrocellulose, and probed for phospho-threonine (Cell Signaling) or total ArfGAP1 using an antibody against the GST tag on the recombinant protein (GST-HRP, Pierce).

Generation of 14-3-3θ transgenic line

Mice were used in accordance with the guidelines of the Association for Assessment and Accreditation of Laboratory Animal Care International (AAALAC) and University of Alabama at Birmingham (UAB) Institutional Animal Care and Use Committee (IACUC). Human 14-3-3θ tagged with an HA epitope tag at the C-terminal end was cloned into a Thy1.2 expression cassette (73) to drive neuronal expression of 14-3-3θ. Following digestion with NdeI and EcoRI, the Thy1.2 construct containing HA-tagged 14-3-3θ was purified and microinjected into C57BL/6 fertilized mouse oocytes. Founder mice were bred with C57BL/6 mice from Jackson labs, and pups were examined for expression of HA-tagged 14-3-3θ in mouse brain by both immunohistochemistry and western blotting. Two of the founder lines showed diffuse neuronal expression of HA-tagged 14-3-3θ (M5 and F1 lines). The M5 line was used for experiments in this paper due to high expression levels in the hippocampus. Hemizygous transgenic mice were identified by genotyping using the following primers: forward primer 5′ ATCTCAAGCCCTCAAGGTAAATG, and reverse primer 5′ CTCCACTTTCTCCCGATAGTCC.

Other mouse lines

BAC wild-type and G2019S-LRRK2 hemizygous transgenic mice (42) were backcrossed on a C57BL/6 background and were bred with wild-type C57BL/6 mice from Jackson labs (Bar Harbor, ME). For experiments evaluating the effect of 14-3-3s on LRRK2, BAC G2019S-LRRK2 hemizygous mice were crossed with hemizygous 14-3-3θ transgenic mice. BAC G2019S-LRRK2 hemizygous mice were also bred with hemizygous difopein-YFP transgenic mice or HA-tagged DN 14-3-3θ mice on a C57BL/6 background obtained from Yi Zhou (40). LRRK2 heterozygous (+/–) knockout mice (19) were crossed with hemizygous difopein or DN 14-3-3 θ mice. BAC R1441G-LRRK2 mice (48) were obtained from Jackson Labs, and a breeding colony was maintained by crossing with FVB/NJ mice, also from Jackson Labs. To test the effect of 14-3-3θ on neurite shortening phenotype of the R1441G-LRRK2 mice, hemizygous R1441G-LRRK2 mice were crossed with hemizygous 14-3-3θ transgenic mice. Only mice from the F1 generation were used for neurite analysis to maintain 50% C57BL/6 and 50% FVB/NJ strain contributions, as the 14-3-3θ mice were created in the C57BL/6 strain and the R1441G-LRRK2 mice were created in the FVB strain.

Primary culture preparation

Hippocampal neurons were isolated from male and female P0 mice. Hippocampi were dissected from individual mice and incubated in papain (Worthington Biochemical, Lakewood, NJ) for 20 min at 37°C. Cells were thoroughly washed using Neurobasal-A media (Thermo Fisher Scientific, Waltham, MA) containing B-27 supplement (Thermo Fisher) and 5% FBS (Sigma) before tituration using fire polished glass pipettes. After centrifugation at 1500*g* for 5 min, pelleted cells were layered on top of a 4% BSA (Jackson ImmunoResearch) in HBSS and centrifuged at 700 rpm for 5 min. Cells were resuspended and plated on 18 mm glass coverslips coated with poly-d-lysine (Sigma). After 16 h, media was removed and replaced by Neurobasal-A media containing B-27 supplement and Arabinose C at 6 µM. Fifty percentage media changes were made every 3 days. For certain experiments, the LRRK2 inhibitor HG-10-102-01 was used to treat cultures at 1.5 µM for the final 48 h in culture prior to immunostaining.

Neurite analysis

At DIV8, cells were fixed in 4% paraformaldehyde and permeabilized with 0.5% Triton X-100. Cells were blocked for a minimum of 1 h with 5% normal goat serum (NGS) in Tris-buffered saline (TBS) and incubated overnight with a primary rabbit antibody against MAP2 (EMD Millipore, Billerica, MA) at 4°C. Cells were rinsed thoroughly with TBS before being incubated with a Cy3-conjugated goat anti-rabbit secondary antibody for 2 h. Cells were again thoroughly washed with TBS before coverslips were mounted on slides using Vectashield mounting solution (Vector Labs, Burlingame, CA). Dendrite lengths were measured using Neurolucida analytical software (MBF Bioscience, Williston, VT).

Immunohistochemistry

Mice were anesthetized with ketamine and xylazine and transcardially perfused with PBS followed by 4% paraformaldehyde in PBS. Brains were dissected, postfixed for 24 h in 4% paraformaldehyde at 4°C, and then placed into a 30% sucrose solution in PBS for 48 h. Brains were sectioned coronally on a Leica microtome with cut thickness of 40 µm. Free floating brain sections were blocked in 10% NGS for 30 min and then incubated overnight with primary mouse anti-HA antibody (1:1000, Sigma) or primary rabbit anti-GFP antibody (1:1000, Abcam), followed by incubation with Cy3-conjugated goat anti-mouse antibody and Alexa-488 conjugated goat anti-rabbit antibody (1:500 Life Technologies)

Statistical analysis

GraphPad Prism 6 (La Jolla, CA) was used for statistical analysis of experiments. Kinase assays, western blot experiments and neurite analyses were analyzed by either Student *t*-test or by one-way ANOVA, followed by *post hoc* pairwise comparisons using Tukey's multiple comparison test.

Supplementary Material

Supplementary Material is available at *HMG* online.

Acknowledgements

We would like to thank Mary Ballestas and the UAB Neuroscience Core Center for preparation of the difopein lentivirus. We also thank Yi Zhou from Florida State University for kindly providing the difopein and 14-3-3θ dominant-negative transgenic mice, Matthew Farrer and Heather Melrose from Mayo Clinic in Jacksonville for kindly providing the BAC G2019S-LRRK2 mice and the LRRK2 knockout mice, and Zhenyu Yuen from the Icahn School of Medicine at Mount Sinai for providing the LRRK2 S935A DNA constructs.

Conflict of Interest statement. Talene Yacoubian declares that she has a US Patent #7,919,262 on the use of 14-3-3s in neurodegeneration.

Funding

This work was supported by the Michael J. Fox Foundation, the American Parkinson Disease Association, the Parkinson's Association of Alabama and National Institutes of Health (R01 NS088533, R01 NS064934 and P30 NS47466).

References

1. Morgan, J.C., Currie, L.J., Harrison, M.B., Bennett, J.P. Jr, Trugman, J.M. and Wooten, G.F. (2014) Mortality in levodopa-treated Parkinson's disease. *Parkinsons Dis.*, **2014**, 426976.
2. Macleod, A.D., Taylor, K.S. and Counsell, C.E. (2014) Mortality in Parkinson's disease: a systematic review and meta-analysis. *Mov. Disord.*, **29**, 1615–1622.
3. Paisan-Ruiz, C., Jain, S., Evans, E.W., Gilks, W.P., Simon, J., van der Brug, M., Lopez de Munain, A., Aparicio, S., Gil, A.M., Khan, N. *et al.* (2004) Cloning of the gene containing mutations that cause PARK8-linked Parkinson's disease. *Neuron*, **44**, 595–600.
4. Zimprich, A., Biskup, S., Leitner, P., Lichtner, P., Farrer, M., Lincoln, S., Kachergus, J., Hulihan, M., Uitti, R.J., Calne, D.B. *et al.* (2004) Mutations in LRRK2 cause autosomal-dominant parkinsonism with pleomorphic pathology. *Neuron*, **44**, 601–607.
5. Healy, D.G., Falchi, M., O'Sullivan, S.S., Bonifati, V., Durr, A., Bressman, S., Brice, A., Aasly, J., Zabetian, C.P., Goldwurm, S. *et al.* (2008) Phenotype, genotype, and worldwide genetic penetrance of LRRK2-associated Parkinson's disease: a case-control study. *Lancet Neurol.*, **7**, 583–590.
6. Correia Guedes, L., Ferreira, J.J., Rosa, M.M., Coelho, M., Bonifati, V. and Sampaio, C. (2010) Worldwide frequency of G2019S LRRK2 mutation in Parkinson's disease: a systematic review. *Parkinsonism Relat. Disord.*, **16**, 237–242.
7. Aasly, J.O., Toft, M., Fernandez-Mata, I., Kachergus, J., Hulihan, M., White, L.R. and Farrer, M. (2005) Clinical features of LRRK2-associated Parkinson's disease in central Norway. *Ann. Neurol.*, **57**, 762–765.
8. Satake, W., Nakabayashi, Y., Mizuta, I., Hirota, Y., Ito, C., Kubo, M., Kawaguchi, T., Tsunoda, T., Watanabe, M., Takeda, A. *et al.* (2009) Genome-wide association study identifies common variants at four loci as genetic risk factors for Parkinson's disease. *Nat. Genet.*, **41**, 1303–1307.
9. Sharma, M., Ioannidis, J.P., Aasly, J.O., Annesi, G., Brice, A., Van Broeckhoven, C., Bertram, L., Bozi, M., Crosiers, D., Clarke, C. *et al.* (2012) Large-scale replication and heterogeneity in Parkinson disease genetic loci. *Neurology*, **79**, 659–667.
10. Simon-Sanchez, J., Schulte, C., Bras, J.M., Sharma, M., Gibbs, J.R., Berg, D., Paisan-Ruiz, C., Lichtner, P., Scholz, S.W., Hernandez, D.G. *et al.* (2009) Genome-wide association study reveals genetic risk underlying Parkinson's disease. *Nat. Genet.*, **41**, 1308–1312.
11. Greggio, E., Jain, S., Kingsbury, A., Bandopadhyay, R., Lewis, P., Kaganovich, A., van der Brug, M.P., Beilina, A., Blackinton, J., Thomas, K.J. *et al.* (2006) Kinase activity is required for the toxic effects of mutant LRRK2/dardarin. *Neurobiol. Dis.*, **23**, 329–341.
12. Lee, B.D., Shin, J.H., VanKampen, J., Petrucelli, L., West, A.B., Ko, H.S., Lee, Y.I., Maguire-Zeiss, K.A., Bowers, W.J., Federoff, H.J. *et al.* (2010) Inhibitors of leucine-rich repeat kinase-2 protect against models of Parkinson's disease. *Nat. Med.*, **16**, 998–1000.
13. Smith, W.W., Pei, Z., Jiang, H., Dawson, V.L., Dawson, T.M. and Ross, C.A. (2006) Kinase activity of mutant LRRK2 mediates neuronal toxicity. *Nat. Neurosci.*, **9**, 1231–1233.
14. West, A.B., Moore, D.J., Choi, C., Andrabi, S.A., Li, X., Dikeman, D., Biskup, S., Zhang, Z., Lim, K.L., Dawson, V.L. *et al.* (2007) Parkinson's disease-associated mutations in LRRK2 link enhanced GTP-binding and kinase activities to neuronal toxicity. *Hum. Mol. Genet.*, **16**, 223–232.
15. Sheng, Z., Zhang, S., Bustos, D., Kleinheinz, T., Le Pichon, C.E., Dominguez, S.L., Solanoy, H.O., Drummond, J., Zhang, X., Ding, X. *et al.* (2012) Ser1292 autophosphorylation is an indicator of LRRK2 kinase activity and contributes to the cellular effects of PD mutations. *Sci. Transl. Med.*, **4**, 164ra161.
16. Caesar, M., Zach, S., Carlson, C.B., Brockmann, K., Gasser, T. and Gillardon, F. (2013) Leucine-rich repeat kinase 2 functionally interacts with microtubules and kinase-dependently modulates cell migration. *Neurobiol. Dis.*, **54**, 280–288.
17. Kett, L.R., Boassa, D., Ho, C.C., Rideout, H.J., Hu, J., Terada, M., Ellisman, M. and Dauer, W.T. (2012) LRRK2 Parkinson disease mutations enhance its microtubule association. *Hum. Mol. Genet.*, **21**, 890–899.
18. Law, B.M., Spain, V.A., Leinster, V.H., Chia, R., Beilina, A., Cho, H.J., Taymans, J.M., Urban, M.K., Sancho, R.M., Ramirez, M.B. *et al.* (2014) A direct interaction between leucine-rich repeat kinase 2 and specific beta-tubulin isoforms regulates tubulin acetylation. *J. Biol. Chem.*, **289**, 895–908.
19. Dachsel, J.C., Behrouz, B., Yue, M., Beevers, J.E., Melrose, H.L. and Farrer, M.J. (2010) A comparative study of Lrrk2 function

in primary neuronal cultures. *Parkinsonism Relat. Disord.*, **16**, 650–655.
20. MacLeod, D., Dowman, J., Hammond, R., Leete, T., Inoue, K. and Abeliovich, A. (2006) The familial Parkinsonism gene LRRK2 regulates neurite process morphology. *Neuron*, **52**, 587–593.
21. Parisiadou, L., Xie, C., Cho, H.J., Lin, X., Gu, X.L., Long, C.X., Lobbestael, E., Baekelandt, V., Taymans, J.M., Sun, L. *et al.* (2009) Phosphorylation of ezrin/radixin/moesin proteins by LRRK2 promotes the rearrangement of actin cytoskeleton in neuronal morphogenesis. *J. Neurosci.*, **29**, 13971–13980.
22. Plowey, E.D., Cherra, S.J. III, Liu, Y.J. and Chu, C.T. (2008) Role of autophagy in G2019S-LRRK2-associated neurite shortening in differentiated SH-SY5Y cells. *J. Neurochem.*, **105**, 1048–1056.
23. Winner, B., Melrose, H.L., Zhao, C., Hinkle, K.M., Yue, M., Kent, C., Braithwaite, A.T., Ogholikhan, S., Aigner, R., Winkler, J. *et al.* (2011) Adult neurogenesis and neurite outgrowth are impaired in LRRK2 G2019S mice. *Neurobiol. Dis.*, **41**, 706–716.
24. Dzamko, N., Deak, M., Hentati, F., Reith, A.D., Prescott, A.R., Alessi, D.R. and Nichols, R.J. (2010) Inhibition of LRRK2 kinase activity leads to dephosphorylation of Ser(910)/Ser(935), disruption of 14-3-3 binding and altered cytoplasmic localization. *Biochem. J.*, **430**, 405–413.
25. Li, X., Wang, Q.J., Pan, N., Lee, S., Zhao, Y., Chait, B.T. and Yue, Z. (2011) Phosphorylation-dependent 14-3-3 binding to LRRK2 is impaired by common mutations of familial Parkinson's disease. *PLoS One*, **6**, e17153.
26. Nichols, R.J., Dzamko, N., Morrice, N.A., Campbell, D.G., Deak, M., Ordureau, A., Macartney, T., Tong, Y., Shen, J., Prescott, A. R. *et al.* (2010) 14-3-3 binding to LRRK2 is disrupted by multiple Parkinson's disease-associated mutations and regulates cytoplasmic localization. *Biochem. J.*, **430**, 393–404.
27. Porter, G.W., Khuri, F.R. and Fu, H. (2006) Dynamic 14-3-3/client protein interactions integrate survival and apoptotic pathways. *Semin. Cancer Biol.*, **16**, 193–202.
28. Dougherty, M.K. and Morrison, D.K. (2004) Unlocking the code of 14-3-3. *J. Cell Sci.*, **117**, 1875–1884.
29. Mackintosh, C. (2004) Dynamic interactions between 14-3-3 proteins and phosphoproteins regulate diverse cellular processes. *Biochem. J.*, **381**, 329–342.
30. Ding, H., Fineberg, N.S., Gray, M. and Yacoubian, T.A. (2013) alpha-Synuclein overexpression represses 14-3-3theta transcription. *J. Mol. Neurosci.*, **51**, 1000–1009.
31. Yacoubian, T.A., Cantuti-Castelvetri, I., Bouzou, B., Asteris, G., McLean, P.J., Hyman, B.T. and Standaert, D.G. (2008) Transcriptional dysregulation in a transgenic model of Parkinson disease. *Neurobiol. Dis.*, **29**, 515–528.
32. Yacoubian, T.A., Slone, S.R., Harrington, A.J., Hamamichi, S., Schieltz, J.M., Caldwell, K.A., Caldwell, G.A. and Standaert, D.G. (2010) Differential neuroprotective effects of 14-3-3 proteins in models of Parkinson's disease. *Cell Death Dis.*, **1**, e2.
33. Slone, S.R., Lavalley, N., McFerrin, M., Wang, B. and Yacoubian, T.A. (2015) Increased 14-3-3 phosphorylation observed in Parkinson's disease reduces neuroprotective potential of 14-3-3 proteins. *Neurobiol. Dis.*, **79**, 1–13.
34. Ulitsky, I., Krishnamurthy, A., Karp, R.M. and Shamir, R. (2010) DEGAS: de novo discovery of dysregulated pathways in human diseases. *PLoS One*, **5**, e13367.
35. Slone, S.R., Lesort, M. and Yacoubian, T.A. (2011) 14-3-3theta protects against neurotoxicity in a cellular Parkinson's disease model through inhibition of the apoptotic factor Bax. *PLoS One*, **6**, e21720.
36. Ding, H., Underwood, R., Lavalley, N. and Yacoubian, T.A. (2015) 14-3-3 inhibition promotes dopaminergic neuron loss and 14-3-3theta overexpression promotes recovery in the MPTP mouse model of Parkinson's disease. *Neuroscience*, **307**, 73–82.
37. Muda, K., Bertinetti, D., Gesellchen, F., Hermann, J.S., von Zweydorf, F., Geerlof, A., Jacob, A., Ueffing, M., Gloeckner, C. J. and Herberg, F.W. (2014) Parkinson-related LRRK2 mutation R1441C/G/H impairs PKA phosphorylation of LRRK2 and disrupts its interaction with 14-3-3. *Proc. Natl. Acad. Sci. USA*, **111**, E34–E43.
38. Masters, S.C. and Fu, H. (2001) 14-3-3 proteins mediate an essential anti-apoptotic signal. *J. Biol. Chem.*, **276**, 45193–45200.
39. Lobbestael, E., Zhao, J., Rudenko, I.N., Beylina, A., Gao, F., Wetter, J., Beullens, M., Bollen, M., Cookson, M.R., Baekelandt, V. *et al.* (2013) Identification of protein phosphatase 1 as a regulator of the LRRK2 phosphorylation cycle. *Biochem. J.*, **456**, 119–128.
40. Qiao, H., Foote, M., Graham, K., Wu, Y. and Zhou, Y. (2014) 14-3-3 proteins are required for hippocampal long-term potentiation and associative learning and memory. *J. Neurosci.*, **34**, 4801–4808.
41. Chan, D., Citro, A., Cordy, J.M., Shen, G.C. and Wolozin, B. (2011) Rac1 protein rescues neurite retraction caused by G2019S leucine-rich repeat kinase 2 (LRRK2). *J. Biol. Chem.*, **286**, 16140–16149.
42. Melrose, H.L., Dachsel, J.C., Behrouz, B., Lincoln, S.J., Yue, M., Hinkle, K.M., Kent, C.B., Korvatska, E., Taylor, J.P., Witten, L. *et al.* (2010) Impaired dopaminergic neurotransmission and microtubule-associated protein tau alterations in human LRRK2 transgenic mice. *Neurobiol. Dis.*, **40**, 503–517.
43. Li, Y., Wu, Y., Li, R. and Zhou, Y. (2007) The role of 14-3-3 dimerization in its modulation of the CaV2.2 channel. *Channels*, **1**, 1–2.
44. Aitken, A. (2002) Functional specificity in 14-3-3 isoform interactions through dimer formation and phosphorylation. Chromosome location of mammalian isoforms and variants. *Plant Mol. Biol.*, **50**, 993–1010.
45. Jones, D.H., Ley, S. and Aitken, A. (1995) Isoforms of 14-3-3 protein can form homo- and heterodimers in vivo and in vitro: implications for function as adapter proteins. *FEBS Lett.*, **368**, 55–58.
46. Sluchanko, N.N. and Gusev, N.B. (2012) Oligomeric structure of 14-3-3 protein: what do we know about monomers? *FEBS Lett.*, **586**, 4249–4256.
47. Yang, X., Lee, W.H., Sobott, F., Papagrigoriou, E., Robinson, C. V., Grossmann, J.G., Sundstrom, M., Doyle, D.A. and Elkins, J. M. (2006) Structural basis for protein-protein interactions in the 14-3-3 protein family. *Proc. Natl. Acad. Sci. USA*, **103**, 17237–17242.
48. Li, Y., Liu, W., Oo, T.F., Wang, L., Tang, Y., Jackson-Lewis, V., Zhou, C., Geghman, K., Bogdanov, M., Przedborski, S. *et al.* (2009) Mutant LRRK2(R1441G) BAC transgenic mice recapitulate cardinal features of Parkinson's disease. *Nat. Neurosci.*, **12**, 826–828.
49. Davies, P., Hinkle, K.M., Sukar, N.N., Sepulveda, B., Mesias, R., Serrano, G., Alessi, D.R., Beach, T.G., Benson, D.L., White, C.L. *et al.* (2013) Comprehensive characterization and optimization of anti-LRRK2 (leucine-rich repeat kinase 2) monoclonal antibodies. *Biochem. J.*, **453**, 101–113.
50. Higashi, S., Moore, D.J., Colebrooke, R.E., Biskup, S., Dawson, V.L., Arai, H., Dawson, T.M. and Emson, P.C. (2007) Expression and localization of Parkinson's disease-associated leucine-rich repeat kinase 2 in the mouse brain. *J. Neurochem.*, **100**, 368–381.
51. West, A.B., Moore, D.J., Biskup, S., Bugayenko, A., Smith, W. W., Ross, C.A., Dawson, V.L. and Dawson, T.M. (2005)

Parkinson's disease-associated mutations in leucine-rich repeat kinase 2 augment kinase activity. *Proc. Natl. Acad. Sci. USA*, **102**, 16842–16847.
52. Webber, P.J., Smith, A.D., Sen, S., Renfrow, M.B., Mobley, J.A. and West, A.B. (2011) Autophosphorylation in the leucine-rich repeat kinase 2 (LRRK2) GTPase domain modifies kinase and GTP-binding activities. *J. Mol. Biol.*, **412**, 94–110.
53. Stafa, K., Trancikova, A., Webber, P.J., Glauser, L., West, A.B. and Moore, D.J. (2012) GTPase activity and neuronal toxicity of Parkinson's disease-associated LRRK2 is regulated by ArfGAP1. *PLoS Genet.*, **8**, e1002526.
54. Xiong, Y., Yuan, C., Chen, R., Dawson, T.M. and Dawson, V.L. (2012) ArfGAP1 is a GTPase activating protein for LRRK2: reciprocal regulation of ArfGAP1 by LRRK2. *J. Neurosci.*, **32**, 3877–3886.
55. Choi, H.G., Zhang, J., Deng, X., Hatcher, J.M., Patricelli, M.P., Zhao, Z., Alessi, D.R. and Gray, N.S. (2012) Brain Penetrant LRRK2 Inhibitor. *ACS Med. Chem. Lett.*, **3**, 658–662.
56. Brunelli, L., Cieslik, K.A., Alcorn, J.L., Vatta, M. and Baldini, A. (2007) Peroxisome proliferator-activated receptor-delta upregulates 14-3-3 epsilon in human endothelial cells via CCAAT/enhancer binding protein-beta. *Circ. Res.*, **100**, e59–e71.
57. Ferguson, A.T., Evron, E., Umbricht, C.B., Pandita, T.K., Chan, T.A., Hermeking, H., Marks, J.R., Lambers, A.R., Futreal, P.A., Stampfer, M.R. *et al.* (2000) High frequency of hypermethylation at the 14-3-3 sigma locus leads to gene silencing in breast cancer. *Proc. Natl. Acad. Sci. USA*, **97**, 6049–6054.
58. Liou, J.Y., Lee, S., Ghelani, D., Matijevic-Aleksic, N. and Wu, K. K. (2006) Protection of endothelial survival by peroxisome proliferator-activated receptor-delta mediated 14-3-3 upregulation. *Arterioscler. Thromb. Vasc. Biol.*, **26**, 1481–1487.
59. Parker, B.S., Cutts, S.M., Nudelman, A., Rephaeli, A., Phillips, D.R. and Sukumar, S. (2003) Mitoxantrone mediates demethylation and reexpression of cyclin d2, estrogen receptor and 14.3.3sigma in breast cancer cells. *Cancer Biol. Ther.*, **2**, 259–263.
60. Wu, J.S., Cheung, W.M., Tsai, Y.S., Chen, Y.T., Fong, W.H., Tsai, H.D., Chen, Y.C., Liou, J.Y., Shyue, S.K., Chen, J.J. *et al.* (2009) Ligand-activated peroxisome proliferator-activated receptor-gamma protects against ischemic cerebral infarction and neuronal apoptosis by 14-3-3epsilon upregulation. *Circulation*, **119**, 1124–1134.
61. Ito, G., Okai, T., Fujino, G., Takeda, K., Ichijo, H., Katada, T. and Iwatsubo, T. (2007) GTP binding is essential to the protein kinase activity of LRRK2, a causative gene product for familial Parkinson's disease. *Biochemistry*, **46**, 1380–1388.
62. Dzamko, N., Inesta-Vaquera, F., Zhang, J., Xie, C., Cai, H., Arthur, S., Tan, L., Choi, H., Gray, N., Cohen, P. *et al.* (2012) The IkappaB kinase family phosphorylates the Parkinson's disease kinase LRRK2 at Ser935 and Ser910 during Toll-like receptor signaling. *PLoS One*, **7**, e39132.
63. Obsilova, V., Kopecka, M., Kosek, D., Kacirova, M., Kylarova, S., Rezabkova, L. and Obsil, T. (2014) Mechanisms of the 14-3-3 protein function: regulation of protein function through conformational modulation. *Physiol. Res.*, **63** Suppl 1, S155–S164.
64. Kajiwara, Y., Buxbaum, J.D. and Grice, D.E. (2009) SLITRK1 binds 14-3-3 and regulates neurite outgrowth in a phosphorylation-dependent manner. *Biol. Psychiatry*, **66**, 918–925.
65. Ramser, E.M., Buck, F., Schachner, M. and Tilling, T. (2010) Binding of alphaII spectrin to 14-3-3beta is involved in NCAM-dependent neurite outgrowth. *Mol. Cell Neurosci.*, **45**, 66–74.
66. Ramser, E.M., Wolters, G., Dityateva, G., Dityatev, A., Schachner, M. and Tilling, T. (2010) The 14-3-3zeta protein binds to the cell adhesion molecule L1, promotes L1 phosphorylation by CKII and influences L1-dependent neurite outgrowth. *PLoS One*, **5**, e13462.
67. Yoon, B.C., Zivraj, K.H., Strochlic, L. and Holt, C.E. (2012) 14-3-3 proteins regulate retinal axon growth by modulating ADF/cofilin activity. *Dev. Neurobiol.*, **72**, 600–614.
68. Marzinke, M.A., Mavencamp, T., Duratinsky, J. and Clagett-Dame, M. (2013) 14-3-3epsilon and NAV2 interact to regulate neurite outgrowth and axon elongation. *Arch. Biochem. Biophys.*, **540**, 94–100.
69. Dhillon, A.S., Meikle, S., Yazici, Z., Eulitz, M. and Kolch, W. (2002) Regulation of Raf-1 activation and signalling by dephosphorylation. *EMBO J.*, **21**, 64–71.
70. Dhillon, A.S., Yip, Y.Y., Grindlay, G.J., Pakay, J.L., Dangers, M., Hillmann, M., Clark, W., Pitt, A., Mischak, H. and Kolch, W. (2009) The C-terminus of Raf-1 acts as a 14-3-3-dependent activation switch. *Cell Signal.*, **21**, 1645–1651.
71. von Kriegsheim, A., Pitt, A., Grindlay, G.J., Kolch, W. and Dhillon, A.S. (2006) Regulation of the Raf-MEK-ERK pathway by protein phosphatase 5. *Nat. Cell Biol.*, **8**, 1011–1016.
72. Wang, X., Wang, Z., Yao, Y., Li, J., Zhang, X., Li, C., Cheng, Y., Ding, G., Liu, L. and Ding, Z. (2011) Essential role of ERK activation in neurite outgrowth induced by alpha-lipoic acid. *Biochim. Biophys. Acta*, **1813**, 827–838.
73. Caroni, P. (1997) Overexpression of growth-associated proteins in the neurons of adult transgenic mice. *J. Neurosci. Methods*, **71**, 3–9.